Drag Reduction in Dilute Flowing Gas-Solid Suspensions

SALVATORE J. ROSSETTI and ROBERT PFEFFER

Department of Chemical Engineering
The City University of New York, New York, N.Y. 10031

The effect of solids loading ratio, particle size, and gas Reynolds number on the pressure drop and flow characteristics of a dilute gas-solid suspension in turbulent pipe flow has been studied experimentally in both vertical and horizontal test sections. Glass beads of 10 to 60μ diameter were used at air Reynolds numbers of 10,000 to 25,000 and solids loading ratios of up to 2.5 Drag reduction was observed in the vertical test section for all of the particles studied, with the 30μ particles yielding a maximum drag reduction of about 75% at a loading ratio of 1.5. In the horizontal test section, drag reduction was observed only with the smallest sized particles, indicating a gravity effect. An explanation of these results based on the particles interacting with the turbulent structure of the gas near the wall has been proposed.

Historically, the first use of gas-solid suspensions occurred in the conveying of food and materials. When the unique contacting properties of suspensions of finely divided materials in a gas became evident, however, their application was no longer limited to conveying materials but spread to include many physical and chemical operations as well. Gas-solid suspensions are now being considered as nuclear reactor coolants and as working fluids in conventional gas power cycles for space power generation.

Even though gas-solid suspensions find such widespread applications, the prediction of pressure losses associated with their flow is still mostly an empirical art. One would expect that as the suspensions become less and less concentrated the flow properties would be more readily characterized and more easily understood, since they approach those of the gas. However, the opposite is true. The flow of dilute gas-solid suspensions is even less predictable than that of concentrated suspensions.

Many analytical approaches attempting to describe the flow characteristics of gas-solid suspensions appear in the literature. Soo and co-workers have studied many different aspects of gas-solid flow, and their work is very valuable in obtaining an insight into some of the complex effects of the interactions of the particles with the flowing gas. A summary of Soo's work as well as many other important contributions to the theory of gas-solid suspension flow can be found in Soo's recent text "Fluid Dynamics of Multiphase Systems" (*25*).

Saffman (*23*) presented the equations of motion of a gas carrying small dust particles and derived the equations satisfied by small disturbances in a steady laminar flow. His analysis indicated that under certain conditions fine dust had a stabilizing action, and that the pressure drop of a suspension could be less than that of a pure gas. Julian and Dukler (*13*) presented correlations for the pressure drop caused by a flowing gas-solid suspension computed by use of an eddy viscosity model. These correlations indicated that the pressure drop of a suspension should monotonically increase as particle concentration increases. Pfeffer, Rossetti, and Lieblein (*21*) applied the Reynolds analogy between heat and momentum transfer to obtain a correlation for the pressure drop associated with flowing suspensions. Boothroyd (*4*) used dimensional analysis in an attempt to understand the flow of suspensions. However, owing to the inherent assumptions necessary with each of the analytical approaches and seemingly conflicting or inadequate experimental results, none of the analyses has proven to be completely adequate.

Experimental investigations with large particles (particle diameter $> 100\ \mu$) (*2, 6, 7, 16, 29, 30*) have found that the addition of solid particles to a turbulently flowing gas will always increase the frictional resistance to flow. Studies with small particles (*10, 14, 15, 20, 24, 28*) have also reported this drag increase. Other investigators using small particles have, however, reported a decrease in the frictional resistance below that of the pure gas at low solids loading ratios (*4, 26, 27*). This phenomenon commonly referred to as *drag reduction* has been found to occur upon the addition of small amounts of viscoelastic material to liquids (*1, 8, 9, 12*) and also in the flow of liquid-solid suspensions (*3, 5*). However, drag reduction with gas-solid suspensions is a dubious phenomenon with meager evidence supporting it.

The objectives of this study were to determine the effects of certain significant variables such as particle concentration (loading ratio), particle diameter, and gas Reynolds number on the pressure drop and flow characteristics of a

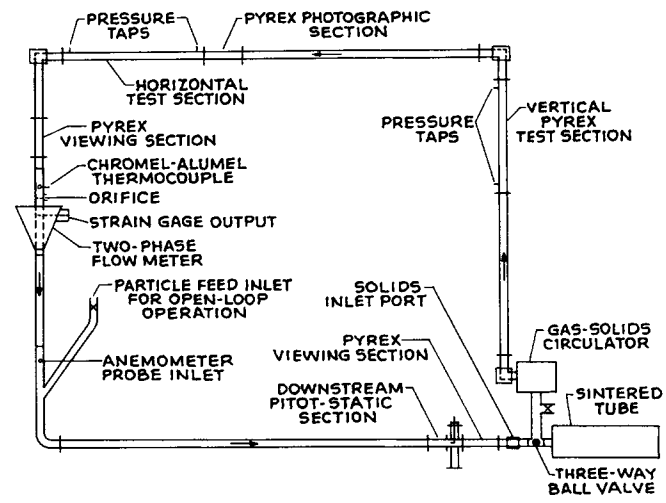

Fig. 1. Schematic diagram of closed loop.

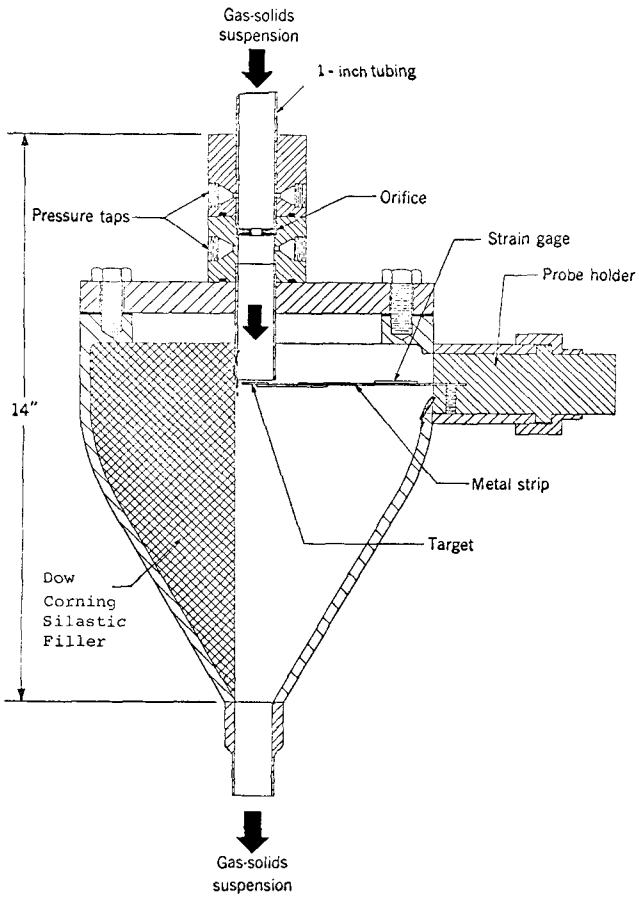

Fig. 2. Two-phase mass flowmeter.

suspension flowing through a tube in fully developed turbulent flow. Particular attention was given to suspensions having a loading ratio of solids to gas flow rates of less than one so as to investigate the extent of drag reduction. In addition, the effect of horizontal or vertical transport of these suspensions was also investigated.

EXPERIMENTAL APPARATUS AND MATERIALS

The apparatus employed in this study was based on the use of a circulating compressor capable of pumping both gas and solids together without damage to its internal parts or causing any contamination of the suspension. This compressor thus permitted design of a closed (recirculating) experimental loop. Pressure drop across both horizontal and vertical test sections were measured by means of micromanometers. Velocity and turbulence measurements were made with an anemometer equipped with a quartz coated thermister probe capable of withstanding the impacts of the solid particles. Particle concentration was determined with a specially designed two-phase mass flowmeter employing strain gauges. In order to properly calibrate the mass flowmeter, the closed loop was modified for open-loop operation. Five different sizes of glass beads were used in the experiments in order to determine the effect of particle diameter on frictional pressure loss.

A schematic diagram of the experimental loop is shown in Figure 1. The loop was primarily constructed of 1 in. O.D. stainless steel tubing but also contained four Pyrex glass viewing sections. Flow is in the counterclockwise direction and is accomplished by the gas-solids circulator which was designed and built by the Franklin Institute and donated to The City College for this research by the Bureau of Mines at Morgantown, West Virginia. The vertical test section was 30 in. long and was located approximately 5 ft. from the elbow in the upward vertical leg of the loop. The horizontal test section was 40 in. long and was preceded by a calming section of approximately 8 ft. in length. The downward vertical leg of the loop contained an

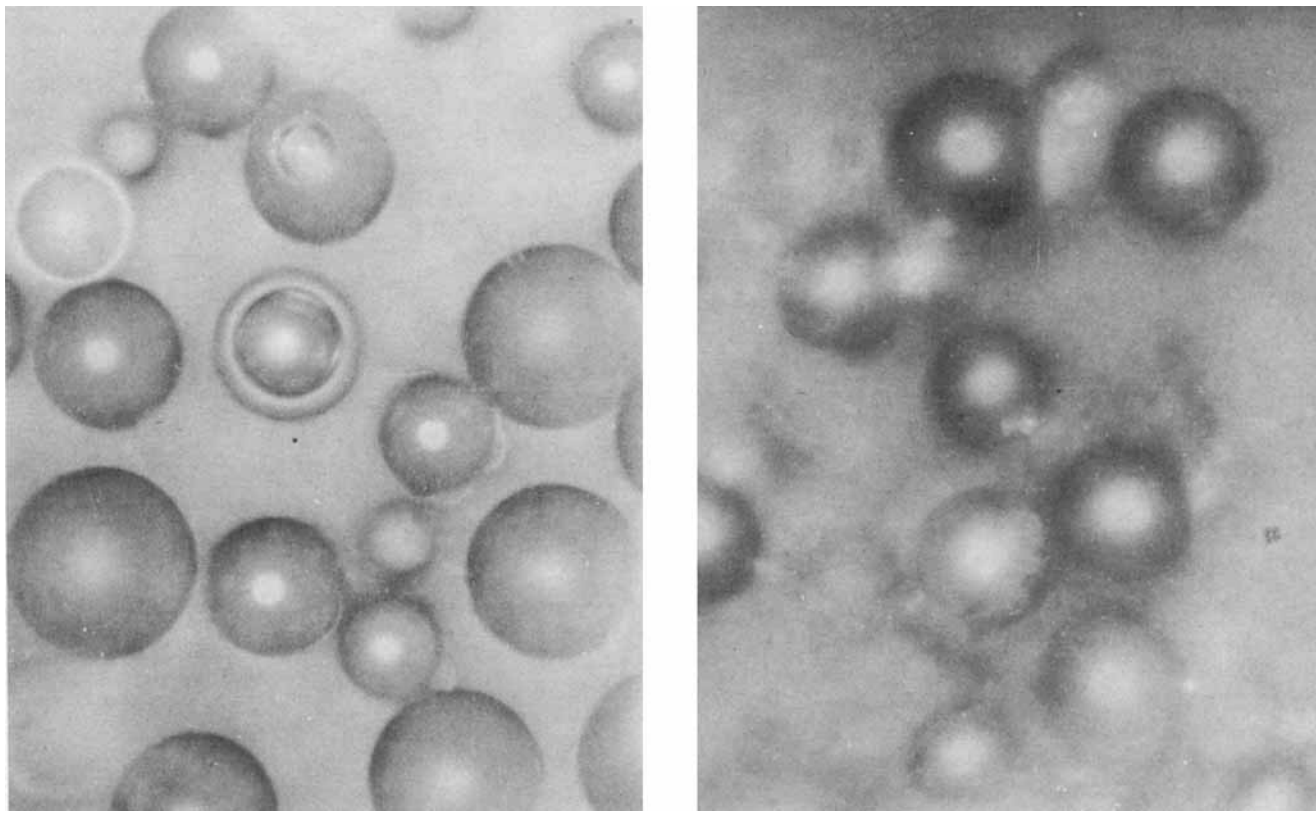

Fig. 3. Microphotographs of 30μ glass beads. (a) Before recirculation—700X magnification. (b) After recirculation for 3480 sec. in the closed loop—700X magnification.

TABLE 1. PARTICLE SIZES

Descriptive title	Actual nominal particle size
50μ	59μ
30μ	34μ
#279	25μ
#981	20μ
#980	10μ

[a] Determined by Coulter counter analysis.

orifice plate, the two-phase flowmeter, and the anemometer probe inlet. A fully detailed description of the experimental loop can be found in reference 22.

A cross section of the two-phase mass flowmeter, designed by the Bureau of Mines, is shown in Figure 2. The metering element is a target attached to a rod at the end of a cantilevered metal strip to which are affixed metal foil strain gauges. The strain gauges sense the deflections of the flexible metal strip caused by the solid and gas acting on the target. The deflection is monitored continuously by a recorder which also continuously monitored the temperature in the loop.

Closed-loop experiments were run with suspensions containing particles of five different particle sizes. These experiments were performed by adding small amounts of particles, usually in 5 or 10 g. increments, to the loop through the opening downstream of the pitot static section in the lower horizontal leg of the loop and then by circulating the particles, taking strain gauge, anemometer, orifice, and vertical and horizontal pressure drop readings. The nominal particle sizes of the five different size glass beads studied are shown in Table 1.

Size distribution analyses were made both photographically and by use of a Coulter counter. Figure 3 shows microphotographs of the 30μ glass beads both before and after circulation through the loop. As can be seen from the figure, the particles are spherical in shape and fairly uniform in size both before and after circulation through the loop.

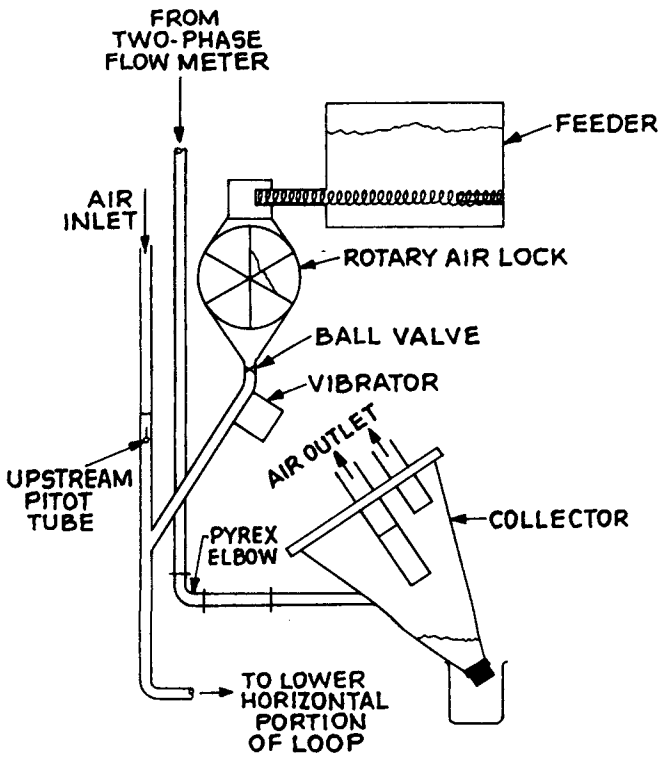

Fig. 4. Schematic diagram of open loop.

CALIBRATION PROCEDURE AND DATA ANALYSIS

In order to obtain meaningful results with the two-phase flowmeter, it first had to be calibrated in an open-loop system under various conditions of solids loading and gas flow rate.

A schematic diagram of the open-loop system used for calibration of the flowmeter is shown in Figure 4. Particles were fed in by using a helix type of volumetric dry feeder into a rotary air lock. The air lock permitted continuous feeding without allowing additional air to be introduced in the system. A vibrator was installed on the inlet Y to maintain continuous flow into the loop. The air velocity was measured by a pitot static tube assembly placed upstream of the particle entrance.

The collector was essentially a cyclone with sintered tubes providing the air outlet. This design prevented solids contamination of the air and also prevented extensive clogging of the sintered tubes. The two-phase flowmeter was calibrated by weighing the particles collected per unit time during open-loop operation. The data obtained were correlated by applying a simple momentum balance.

The strain gauge reading obtained from the two-phase flowmeter is proportional to the force which the fluid exerts on the circular target inserted in the stream. This force is equal to the time rate of change of momentum of the suspension, so that in the absence of slip between the particles and the gas and no acceleration effects

$$V_{ST} = K_1 \rho_1 v_g (\rho_g v_g) + K_2 \rho_g v_g (w_p) \qquad (1)$$

Since the area of the target does not occupy the entire flow area of the tube, it is entirely possible that the relations between V_{ST} and the mass flow rate of gas and solids is not linear, so that an equation of the form

$$V_{ST} = K_1 (\rho_g v_g)(\rho_g v_g)^a + K_2 (\rho_g v_g)(w_p)^b \qquad (2)$$

may be expected. The experimental data were found to fit Equation (2) very well, and best values of the constants were determined to give

$$V_{ST} = 0.0128 (\rho_g v_c)(\rho_g v_c)^{0.808} + 0.0155 (\rho_g v_c)(w_p)^{0.808} \qquad (3)$$

where v_c, the center line gas velocity has been used to replace v_g, the average gas velocity for convenience purposes. It is interesting to note that the constants a and b were both found to have the same value. Since the loading ratio η is defined as the ratio of the particle flow rate W_p and the gas mass flow rate $0.8 \rho_g v_c A$, the final correlation can be expressed in terms of η as

$$\eta = \left[\frac{V_{ST}}{0.0217 (\rho_g v_c)^{1.808}} - 0.590 \right]^{1.238} \qquad (4)$$

Although technically valid only for the 30μ particles which were used in the calibration runs, this correlation was used to determine loading ratios for all the glass particles studied in this work.

After calibration of the two-phase flowmeter, attention was turned to running the closed-loop experiments. In order to make sure that fully developed flow was obtained in both horizontal and vertical sections, velocity profiles and pressure drops were taken with air used as the flowing fluid. The thermistor anemometer probe which was used to determine gas velocity profiles during closed-loop operation with suspensions was also calibrated against the pitot tube in the lower horizontal section, as was the orifice upstream of the two-phase flowmeter.

Velocity profiles and friction factor data were obtained for tube Reynolds numbers between 10,000 and 40,000. The gas velocity profile data agreed with predicted profiles with the $1/7^{th}$ power law based on the experimentally determined center line velocity to within 3%. Experimentally measured friction factors in the horizontal test section were compared with the recommended correlation (*11*)

$$f = 0.184 N_{Re}^{-0.2} \qquad (5)$$

and were found to be within ± 5%. The vertical test section data seemed to fit the other recommended correlation (*11*)

$$f = 0.0056 + 0.5 N_{Re}^{-0.32} \qquad (6)$$

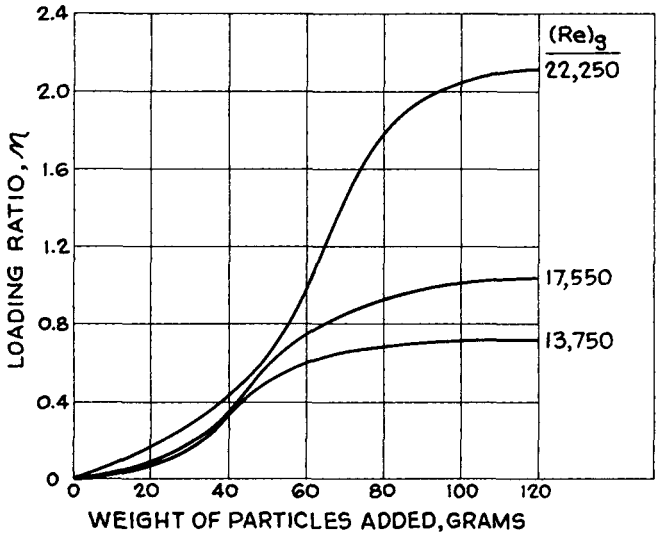

Fig. 5. Loading ratio as function of weight of 30μ particles added to closed loop.

slightly better; again the agreement was found to be within $\pm$ 5% of the correlation.

After the calibration and pure gas runs were completed, data were collected for suspensions flowing in the closed loop. Friction factors for both suspension flow and pure gas flow were calculated by using the common relation for incompressible gas flow

$$f = \frac{2\, g_c \Delta P D}{\rho_g \bar{v}^2 L} \tag{7}$$

where the friction factor is calculated by using the gas density and an average gas velocity ($\bar{v} = 0.8\, v_c$) for each case. Since the pressure drop is very small compared with the static pressure, and because the loop flow is essentially isothermal, acceleration effects are negligible and

$$\Delta P = \Delta P_m \tag{8}$$

for the horizontal test section and

$$\Delta P = \Delta P_m - \eta \rho_g L \tag{9}$$

for the vertical test section, where ΔP_m is the measured pressure drop. The friction factors calculated by these relations for the suspension were then divided by friction factors calculated by Equation (5) for horizontal test section data and Equation (6) for vertical test section data at the same gas Reynolds number. The friction factor ratio for the horizontal section, therefore, represents the ratio of suspension to air pressure drop at a given Reynolds number. For the vertical test section this friction factor ratio is the pressure drop ratio corrected for the solids head in this section.

EXPERIMENTAL RESULTS

During closed-loop experimental operations with a suspension as the working fluid, mass flow ratios, friction factors for both vertical and horizontal test sections, center line velocity, and percent turbulence as well as orifice coefficients were determined. In addition, a photographic analysis with the Pyrex section preceding the horizontal test section was performed for representative Reynolds number and loading ratio conditions. Particle size distribution analyses were also made on representative particulate samples both before and after circulation through the loop. The results of these analyses and experiments are presented and discussed below.

Curves of loading ratio as a function of weight of particles added to the system were obtained for the five particle sizes at each of three different Reynolds number ranges. These are shown in Figure 5 for the 30μ particles and are typical of the type of results obtained with all but the smallest particles. For each particle size a comparison of the plots for the three different Reynolds numbers showed that the higher the Reynolds number the higher the loading ratio at any given weight added to the system. The effect is more pronounced as the weight added to the loop increases, indicating that a larger percentage of particles are entrained by the gas when its velocity is high as compared with when it is low.

The shape of these curves can be explained on the basis of differing interacting effects. The lower portion of the curves is less steep and indicates that a small percentage of the particles added to the system are actually circulating. For the larger particles this effect was more pronounced than for smaller particles and is primarily due to the particles accumulating in irregularities in the loop. For the smaller particles the effect can also be attributed to their cohesiveness which initially makes them more difficult to circulate and possibly indicates a tendency for particles to coat the surface of the loop (although this was not visually observed except for the smallest size glass beads). The steep portion of the curves appears to occur after the surface irregularities are filled and after cohesive forces are no longer sufficient to prevent additional particles from being circulated.

After this steep portion, the figure indicates a second flattened part of the curves. In this region adding more particles to the system does not appear to significantly increase the amount of circulating material. This is a result of particle sedimentation, so that as particles are added other parti-

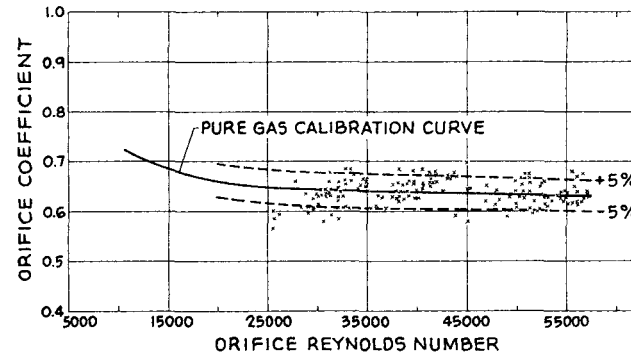

Fig. 6. Orifice coefficient as function of orifice Reynolds number for all particle sizes and loading ratios.

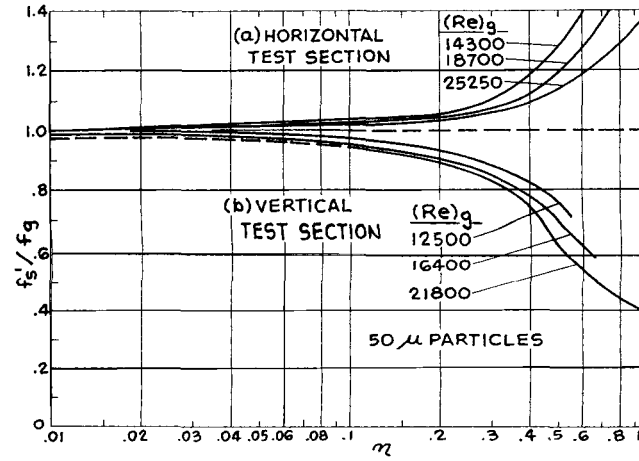

Fig. 7. Friction factor ratio as function of loading ratio with Reynolds number as parameter for 50μ particles.

cles settle out at approximately the same rate. This sedimentation can be partially attributed to the size of the particles, as the 50μ particles exhibit this second flattened portion of the curve at the lowest concentration for the highest Reynolds number studied. However, since this flattening out occurs at approximately the same loading ratio (at a given Reynolds number) for the other particles, and since at the lower Reynolds numbers the smaller particles exhibited flat portions at the same or lower concentration than the large particles, a more complicated explanation is indicated. The cohesiveness of the fine particles almost certainly will tend to cause sedimentation at lower concentration than would be otherwise expected. Furthermore, the lower the velocity the more important the cohesive force, since reentrainment in the fluid stream becomes more difficult.

The smallest particles (#980 glass beads) did not exhibit the above behavior. The curves obtained for these particles were extremely flat, indicating difficulty of entrainment. Furthermore, it was also found that with these particles humidity strongly affected the loading ratio obtained at a given weight added to the system. At high humidity few particles could be circulated at any but the highest Reynolds number. These results tend to confirm that particle cohesiveness plays an important role in determining loading ratio characteristics.

Orifice coefficients were also calculated for all of the closed-loop runs at different particle loading ratios and Reynolds numbers. These results are plotted in Figure 6 along with a curve representing the orifice calibration obtained with pure air as the circulating fluid. Dashed curves representing a $\pm$ 5% deviation from this curve are also shown. Since very few data points fall outside of these dashed curves, it appears that the orifice coefficient was not affected by the presence of particles in the flow stream. These results confirm Orr's contention (17) that a properly calibrated orifice can be used to determine gas mass flow rates for dilute suspensions.

The pressure drop data obtained were analyzed by plotting the ratio of the friction factor with and without particles at the same gas Reynolds number as a function of solids loading ratio for both the horizontal and vertical test sections for each of the five particle sizes and each of three

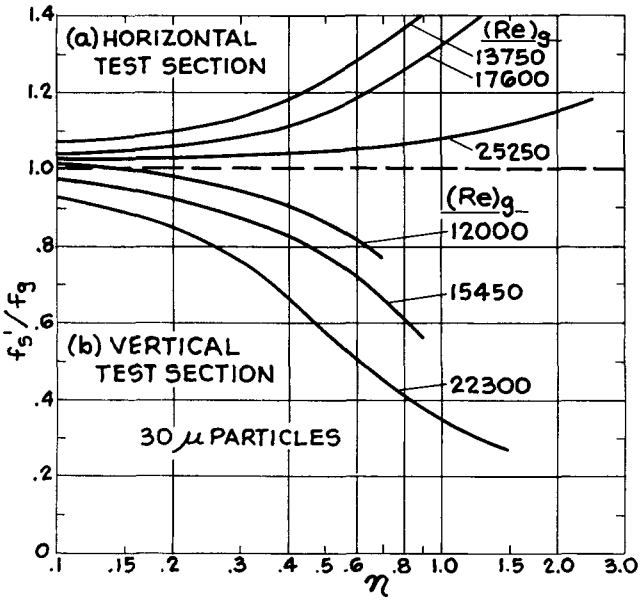

Fig. 8. Friction factor ratio as function of loading ratio with Reynolds number as parameter for 30μ particles.

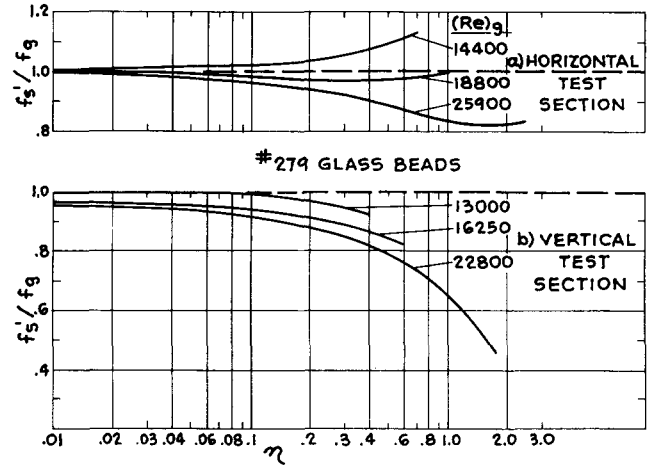

Fig. 9. Friction factor ratio as function of loading ratio with Reynolds number as parameter for # 279 glass beads.

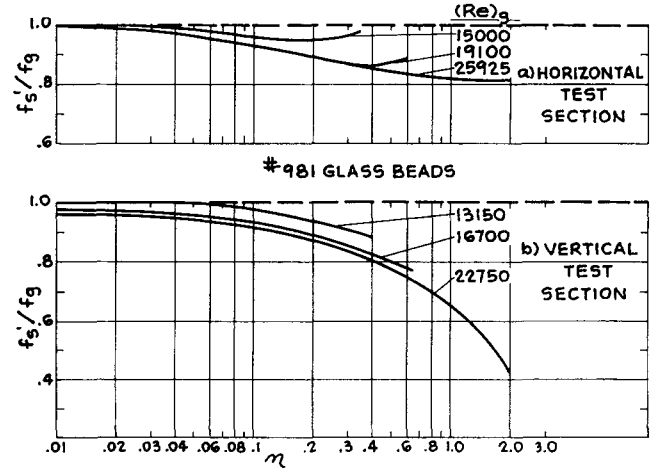

Fig. 10. Friction factor ratio as function of loading ratio with Reynolds number as parameter for # 981 glass beads.

Reynolds number ranges studied. A great deal of data were taken, and although the points showed quite a bit of scatter (all of the data points can be found in reference 22), curves were faired in by eye to represent the data.

Figure 7 shows the curves thus obtained for the 50μ particles. The figure shows an increase in the friction factor ratio as the loading ratio increased for each Reynolds number in the horizontal test section. The largest increase occurred at the lowest Reynolds number. In the vertical test section the curves show a large decrease in friction factor ratio as loading ratio is increased. The drag reduction is found to be greatest at the highest Reynolds number. The figure also indicates that at the higher Reynolds number the friction factor ratio appears to have an inflection, perhaps indicating a tendency to reach a minimum.

The results obtained by using the 30μ particles appear to exhibit similar trends as shown by Figure 8. The figure indicates less drag increase in the horizontal test section and slightly greater drag reduction in the vertical section at the highest Reynolds number considered.

The results with the #279 glass beads shown in Figure 9 indicate that with these particles drag reduction is also found in the horizontal section at the two highest Reynolds numbers. However, the decrease is at most 18%, and there is a slight drag increase at the lowest Reynolds number condition. The results in the vertical test section again indicate drag reduction, but not to the same extent as with the larger particles. No inflection was observed for the verti-

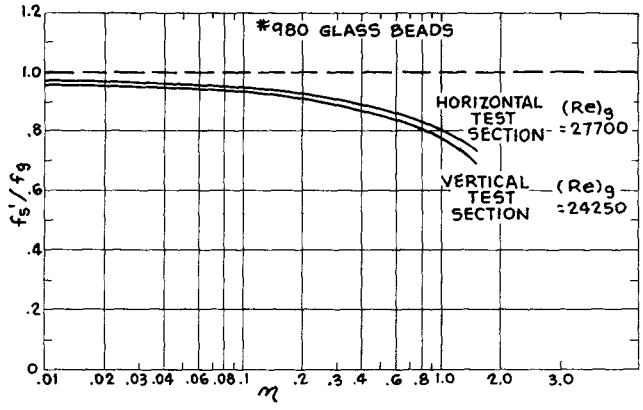

Fig. 11. Friction factor ratio as function of loading ratio with Reynolds number as parameter for #980 glass beads.

cal test section results up to the highest loading ratio investigated.

The #981 glass beads were very similar to the #279 beads, having a mean diameter of 20μ compared with 25μ for the #279 beads. However, the #981 beads had a somewhat different size distribution. In view of their size similarity, it was not surprising that the results for the #981 glass beads in both the horizontal and vertical test sections as shown in Figure 10 exhibited the same general trends and magnitudes as those for the #279 glass beads. The only exception to this agreement appears in the horizontal data at the lowest Reynolds number, where a slight drag reduction rather than a slight drag increase is shown. This could be attributed to the fact that the #279 glass beads contained more larger particles than the #981 beads. This is also the probable reason that all of the horizontal test section friction factor results are slightly lower than for the #279 glass beads.

The smallest particles used in this investigation were the #980 glass beads (average $D_p = 10\mu$). The results with these particles showed practically no effect of Reynolds number. As seen in Figure 11, these particles gave slight drag reduction in both horizontal and vertical test sections. Furthermore, there appears to be practically no difference in the results for both the horizontal and vertical test sections.

DISCUSSION OF RESULTS

The best explanation for the vertical test section results appears to be given by a theoretical analysis on the stability of a dusty gas by Saffman (23). In this analysis, Saffman showed that if the particles are fine enough for the relaxation time, which is a measure of the rate at which the velocity of a particle adjusts to changes in the gas velocity, to be small compared with the time scale of the turbulent eddies, then the addition of particles causes the critical Reynolds number for transition from laminar to turbulent flow to be decreased, and a drag increase results which is proportional to the increased density of the fluid. However, he predicts that if the particles are coarse so that the relaxation time is relatively large, then the suspension has a stabilizing action (the particles cause a higher critical Reynolds number and less frictional pressure loss). In other words, the finite slip velocity between the particles and the gas causes an extra dissipation which extracts energy from the turbulence and presumably damps it, thereby reducing the Reynolds' stresses and the pressure loss. As indicated by the work of Soo (25), this mechanism would be especially pronounced in the vicinity of the wall, where the velocity of the particles greatly exceeds that of the gas.

From Saffman's analysis it would be expected that the larger particles which lag behind the turbulent fluctuations of the flowing air will yield more drag reduction than smaller particles, which to some extent follow the turbulent fluctuations of the fluid. The fact that the 50μ particles yield slightly less drag reduction than the 30μ particles in the vertical test section is also reasonable, since, according to this model, increasing the size of particles already having a relaxation time very much greater than the characteristic time scale of the eddies lessens the stabilizing effect at a given particle concentration. At the gas Reynolds numbers studied in this investigation, it would appear that the 30μ particles yield the optimum relaxation time, since both larger and smaller sized particles result in less drag reduction.

The results for the horizontal test section cannot be fully explained on the basis of the theory just presented. The reason for this is apparently due to gravitational effects which cause the particle number density to vary across the tube and not remain constant as required by Saffman's analysis. Because of gravity, the larger particles tend to congregate in the lower half of the horizontal section. As the particles become smaller, their sedimentation velocity decreases, hence decreasing the tendency toward segregated flow resulting in the friction factor ratios for the two sections to approach one another. The fact that the smallest particles used in this study yielded essentially the same results in the horizontal and vertical test sections seems to confirm this theory. With the larger (50μ and 30μ) particles a drag increase was observed in horizontal flow which may be attributed to the fact that many of these particles were transported through the horizontal sections in bouncing flow, that is, by bouncing along the bottom of the tube. This bouncing flow caused additional frictional pressure drop. Since the number density of the particles is not uniform, the upper portion of the horizontal section is less affected by the particulate flow, so that the net result is a drag increase for these larger particles. As the particles become smaller the segregated flow is minimized and drag reduction results.

These concepts can perhaps be best illustrated by a numerical example. The relaxation time of the particles is calculated as the ratio of the momentum of the particle to the force exerted on it. Assuming that the particles are spheres of diameter D_p, and using Stokes' drag formula, we get

$$t_R = \frac{1}{18} D_p^2 \rho_p/\mu \qquad (10)$$

The characteristic time for energy containing eddies may be expressed as (29)

$$t_e = 0.1\ D/2U_\tau \qquad (11)$$

where U_τ is the conventional friction velocity, and the characteristic time for large eddies is

$$t_l = D/2U_\tau \qquad (12)$$

The effect of gravity will make itself felt when the terminal settling velocity of the particle is of the same order of magnitude as the friction velocity; again the terminal settling velocity may be determined by using Stokes' law expression.

Table 2 lists the calculated relaxation time and terminal velocity of the five different size particles. This table will be used in conjunction with calculations made by using a typical set of experimental data as indicated below:

Data:

$\overline{v} = 44.5$ ft./sec.
$\Delta P = 1.737$ lb./sq.ft.
$\rho_g = 0.0790$ lb./cu.ft.
$(N_{Re})_g = 24{,}650$
$D = 0.0833$ ft.
$L = 2.5$ ft.

Calculated results: $U_\tau = 2.43$ ft./sec.
$t_e = 0.0017$ sec.
$t_l = 0.017$ sec.

Referring to the calculated relaxation times for the various sized particles in Table 2, one would expect, on the basis of Saffman's theory, that drag reduction would occur in the vertical section for this Reynolds number condition for each of the particles since the relaxation times are all greater than t_e. However, it would also be expected that the magnitude of this drag reduction would be smallest for the #980 glass beads where t_R is only slightly greater than t_e. It would also be expected that the maximum drag reduction would occur for particles sized somewhere between the #279 and 30μ particles and decrease for larger sized particles where $t_R > t_l$. These observations are in good agreement with the experimental results for the vertical test section. Results for the horizontal section are complicated by the effect of gravity. The third column of Table 2 indicates

Table 2. Particle Relaxation Time and Terminal Velocity

Particle size	Relaxation time	Terminal velocity
#980 (10μ)	0.0026 sec.	0.084 ft./sec.
#981 (20μ)	0.010 sec.	0.332 ft./sec.
#279 (25μ)	0.015 sec.	0.483 ft./sec.
30μ (34μ)	0.031 sec.	1.01 ft./sec.
50μ (59μ)	0.094 sec.	3.02 ft./sec.

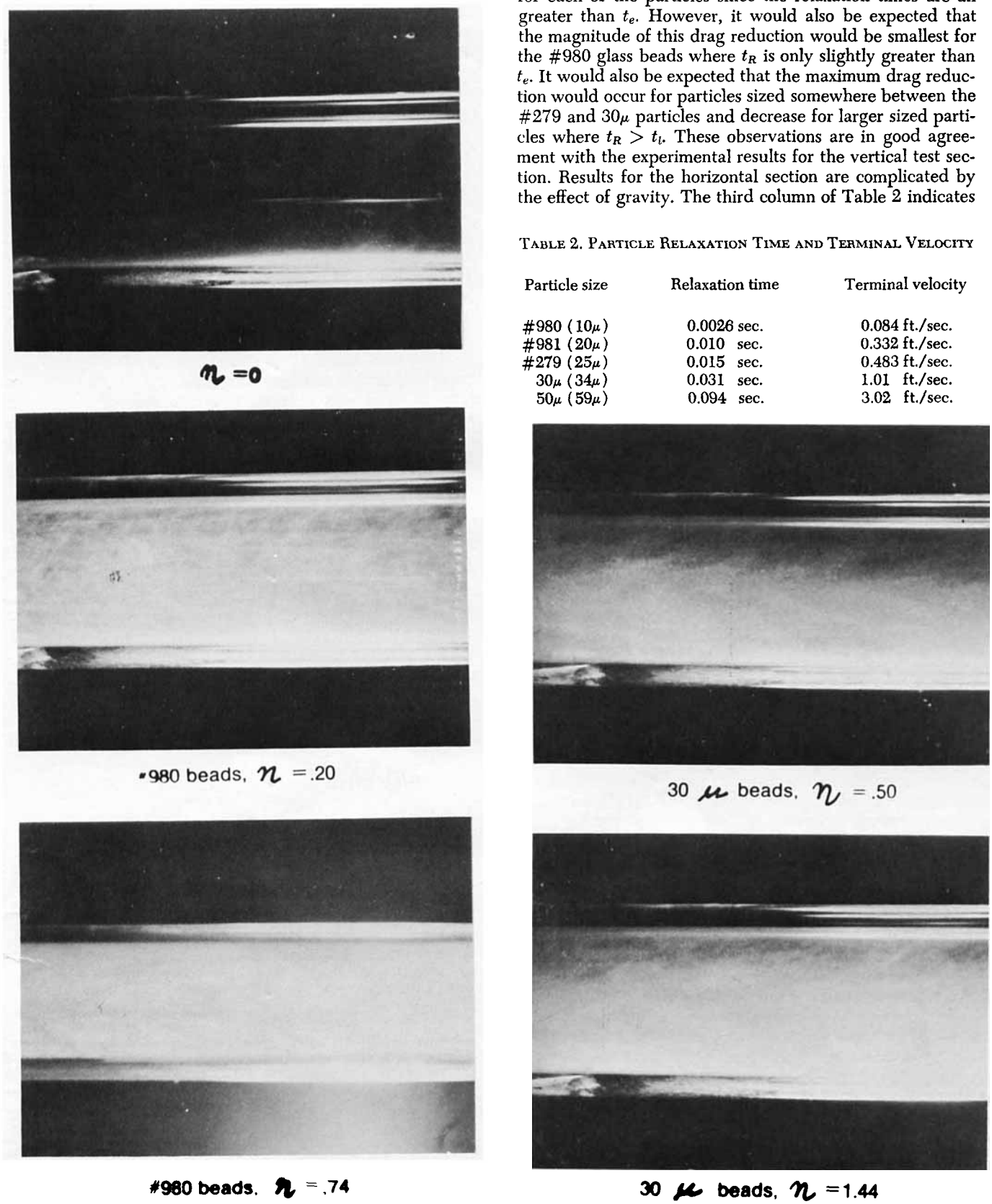

Fig. 12. Gross flow photographs

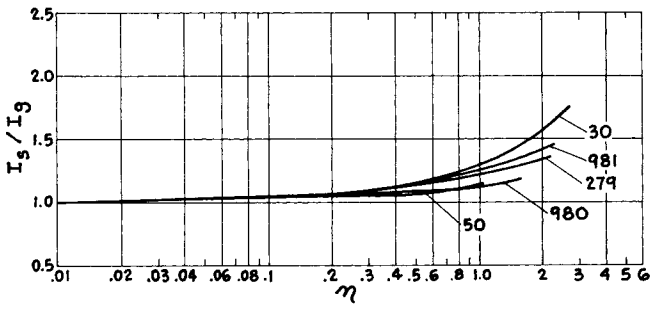

Fig. 13. Relative turbulence intensity ratio as function of loading ratio.

that the effect of gravity will become prominent for the 30 and 50μ particles where the terminal and friction velocities are of the same order of magnitude. This again is in agreement with the observed results.

Photographs showing the gross flow patterns of the particles under varying conditions of loading and Reynolds number appear to confirm the fact that the smaller particles respond to the turbulent fluctuations of the fluid to a greater extent than the larger particles. Figure 12 shows the gross flow patterns for the #980 glass beads and the 30μ glass beads at two different loading conditions. Here the light areas represent particles. For the small particles it can be seen by the wispiness of this particulate flow that many of the particles are responding to the turbulent fluctuations of the fluid. The photographs of the 30μ glass beads indicate very few of these wisps and also clearly show the segregated flow exhibited in the horizontal section for these particles.

In an effort to clarify some aspects of the drag reduction experimentally, preliminary measurements of the intensity of turbulence were taken at the center of the vertical test section by using the thermistor anemometer probe. Figure 13 shows variation of intensity of turbulence ratio with and without particles as a function of loading ratio for each of the five particles studied. These results are somewhat paradoxical in that the ratio of the intensity of turbulence with particles to that of particle free air was found to increase as the particles were added, with the largest increase shown by the 30μ particles which also gave the largest drag reduction. On the basis of the theory presented above, it was expected that these particles would show the largest decrease in the intensity of turbulence. However, it may be that the interaction of the particles with the turbulence eddies occurs very close to the wall and, that, at the center, the intensity of turbulence is actually greater. Similar results have been found with drag reducing liquids (*19*), but it is obvious that many more turbulent intensity measurements must be taken before any reasonable conclusion can be made from these measurements.

CONCLUDING REMARKS

This experimental investigation has shown some remarkable effects of the influence of small particle loadings and different particle size on the pressure drop and flow characteristics associated with turbulent gas-particle flow in a tube. The phenomenon of drag reduction has been found to occur under certain flow conditions in both vertical and horizontal test sections. At a loading ratio of 1.5 and a gas Reynolds number of 25,000, for example, the friction factor ratio in the vertical test section was found to be as low as 0.27 when transporting 30μ particles in air. This indicates a reduction in drag of close to 75%! An explanation of these results based on the interaction of the particles with the turbulent structure of the fluid in the vicinity of the wall has been proposed. Additional study, both experimental and theoretical, is in progress to clarify these results even further and to discover how they may be applied to advantage in industrial processes.

ACKNOWLEDGMENT

The support of this research by the National Aeronautics and Space Administration under Grant NGR-33-013-029 is gratefully acknowledged. The authors also wish to thank the Bureau of Mines for the donation of the gas-solids circulator and two-phase flowmeter, and E. I. duPont deNemours Company for performing the particle size distribution analyses.

NOTATION

A = cross-sectional area of tube, sq.ft.
a, b = constants in Equation (2)
D = tube diameter, ft.
D_p = particle diameter, μ or ft.
f = Blasius friction factor, dimensionless
g_c = gravitational constant, $(\text{lb.}_m)(\text{ft.})/(\text{lb.}_f)(\text{sec.}^2)$
K_1, K_2 = constants in Equation (1)
I = intensity of turbulence, dimensionless
L = length of test section, ft.
N_{Re} = gas Reynolds number, dimensionless
ΔP = pressure drop across test section, lb._f/sq.ft.
ΔP_m = measured pressure drop, lb._f/sq.ft.
t = time, sec.
t_e = eddy characteristic time, sec.
t_l = large eddy characteristic time, sec.
t_R = relaxation time, sec.
U_τ = friction velocity, ft./sec.
$\bar{v}$ = average velocity of gas, ft./sec.
v_c = centerline gas velocity
v_s = velocity of suspension, ft./sec.
V_{ST} = strain gauge output, mv.
W_p = particle flow rate, g./sec.
ρ_g = gas density, lb./cu.ft.
ρ_p = particle density, lb./cu.ft.
η = loading ratio, particle mass flow rate/gas mass flow rate, dimensionless
μ = gas viscosity, lb./ft.-sec.

Subscripts

g = gas
p = particles
s = suspension

LITERATURE CITED

1. Astarita, G., *Ind. Eng. Chem. Fundamentals,* **4,** 354 (1965).
2. Belden, D. H., and L. S. Kassel, *Ind. Eng. Chem.,* **41,** 1174 (1949).
3. Bobkowicz, A. J., and W. H. Gauvin, *Can. J. Chem. Eng.,* **43,** 87 (1965).
4. Boothroyd, R. G., *Trans. Inst. Chem. Engrs.,* **44,** 306 (1966).
5. Daily, J. W., and G. Bugliarello, *Tappi,* **44,** 497 (1961).
6. Dogin, M. E., and V. P. Lebedev, *Intern. Chem. Eng.,* **2,** 64 (1962).
7. Doig, I. A., and G. H. Roper, *Ind. Eng. Chem. Fundamentals,* **6,** 247 (1967).
8. Ernst, W. D., *AIChE J.,* **12,** 581 (1966).
9. Fabula, A. G., *Proc. Fourth Intern. Congr. Rheol.,* 455 (1965).
10. Farber, L., *Ind. Eng. Chem.,* **41,** 1184 (1949).
11. Foust, A. S., L. A. Wenzel, C. W. Clump, L. Maus, and L. B. Andersen, "Principles of Unit Operations," Wiley, New York (1960).
12. Hershey, H. C., and J. L. Zakin, *Ind. Eng. Chem. Fundamentals,* **6,** 381 (1967).
13. Julian, F. M., and A. E. Dukler, *AIChE J.,* **11,** 853 (1965).

14. McCarthy, H. E., and J. H. Olson, *Ind. Eng. Chem. Fundamentals*, **7**, 471 (1968).
15. Mehta, N. C., J. M. Smith, and E. W. Comings, *Ind. Eng. Chem.* **49**, 986 (1957).
16. Mitlin, L., PhD. thesis, Univ. London, England (1954).
17. Orr, C., "Particulate Technology," MacMillan, New York (1966).
18. Owen, P. R., *J. Fluid Mech.*, **39**, Part 2, 407-432 (1969).
19. Paterson, G. K., Ph.D. thesis, Univ. Missouri, Rolla (1966).
20. Peskin, R. L., Quarterly Reports 63-1 and 64-1, Contract No. AT (30-1) 2930, Rutgers Univ., New Brunswick, N. J. (1963).
21. Pfeffer, R., S. J. Rossetti, and S. Lieblein, *NASA TN D3603* (1966).
22. Rossetti, S. J., Ph.D. thesis, City Univ. of N. Y. (1969).
23. Saffman, P. G., *J. Fluid Mech.*, **13**, 120 (1962).
24. Schluderberg, D. C., R. L. Whitelaw, and R. W. Carlson, *Nucleonics*, **19**, 67 (1961).
25. Soo, S. L., "Fluid Dynamics of Multiphase Systems," Blaisdell Publishing Co. (1967).
26. ———, and G. J. Trezek, *Ind. Eng. Chem. Fundamentals*, **5**, 388 (1965).
27. Sproull, W. T., *Nature*, **190**, 976 (1961).
28. Tien, C. L., and V. Quan, *Paper No. 62-HJ-15 ASME* (1962).
29. Vogt, E. G., and R. R. White, *Ind. Eng. Chem.*, **40**, 1731 (1948).
30. Wen, C. Y., and H. P. Simons, *AIChE J.*, **5**, 263 (1959).

Manuscript received August 4, 1970; revision received April 26, 1971; paper accepted April 28, 1971. Paper presented at AIChE Puerto Rico meeting.

Surface Diffusion of Adsorbable Gases Through Porous Media

L. A. ROYBAL and S. I. SANDLER

Department of Chemical Engineering
University of Delaware, Newark, Delaware 19711

An activated diffusion, or site-hopping, mechanism is used to describe surface diffusion of gases through porous media. This analysis provides a useful and accurate method for correlating data at submonolayer coverages on energetically heterogeneous surfaces. The data needed to use this correlation are surface area and pore structure of the adsorbent, adsorption isotherms at two or more temperatures, and the activation energy for migration. The former quantities are easily determined from Knudsen diffusion and adsorption measurements, while the activation energy can be found from a single permeability measurement. Predictions made in this way show excellent agreement with experimental data.

Surface diffusion plays an important role in the transport of gases through beds of porous and nonporous solids. It has been measured for a number of gases to (*1* to *10*), and attempts to find a mathematical description of this phenomenon have been made. An excellent review of early developments in adsorption and surface diffusion studies is presented by Dacey (*11*). Our objective is to find a plausible explanation for the fundamental surface transport mechanism and to use this model to correlate data covering broad ranges of temperature, surface properties, and gas-solid systems.

THEORY

The activated, or site-hopping, mechanism is commonly used to describe submonolayer surface diffusion (*1*, *4*, *12* to *14*). It postulates that an adsorbed molecule must partially desorb to migrate from one localized site to another. At room temperature, an adsorbed molecule may make as many as 6,000 jumps before completely desorbing (*15*). If one assumes a migrating molecule is more likely to readsorb at a vacant site than at an occupied site (*16*), a net flux of hopping molecules in the direction of decreasing surface concentration results.

Weaver and Metzner (5) derived an expression that relates the rate of surface diffusion to the pressure gradient within a cylindrical porous pellet. Their result is

$$I = \frac{s\rho}{2\pi j^2}\left[r\frac{\partial\overline{\lambda^2}}{\partial P} + \frac{\pi}{2j}\overline{\lambda^2}\frac{\partial r}{\partial P}\right] \qquad (1)$$

Here s is the specific surface area of the solid, j is the tortousity factor, ρ is the adsorbate density, $\overline{\lambda^2}$ is the average value of the square of the migration distance, r is the rate of migration, P is pressure, and I the permeability. This expression can be used to correlate experimental data or predict surface diffusion rates if the quantities $\overline{\lambda^2}$, $\frac{\partial\overline{\lambda^2}}{\partial P}$,

Correspondence concerning this paper should be addressed to Stanley I. Sandler. L. A. Roybal is with E. I. duPont de Nemours & Company, Wilmington, Delaware.